Report
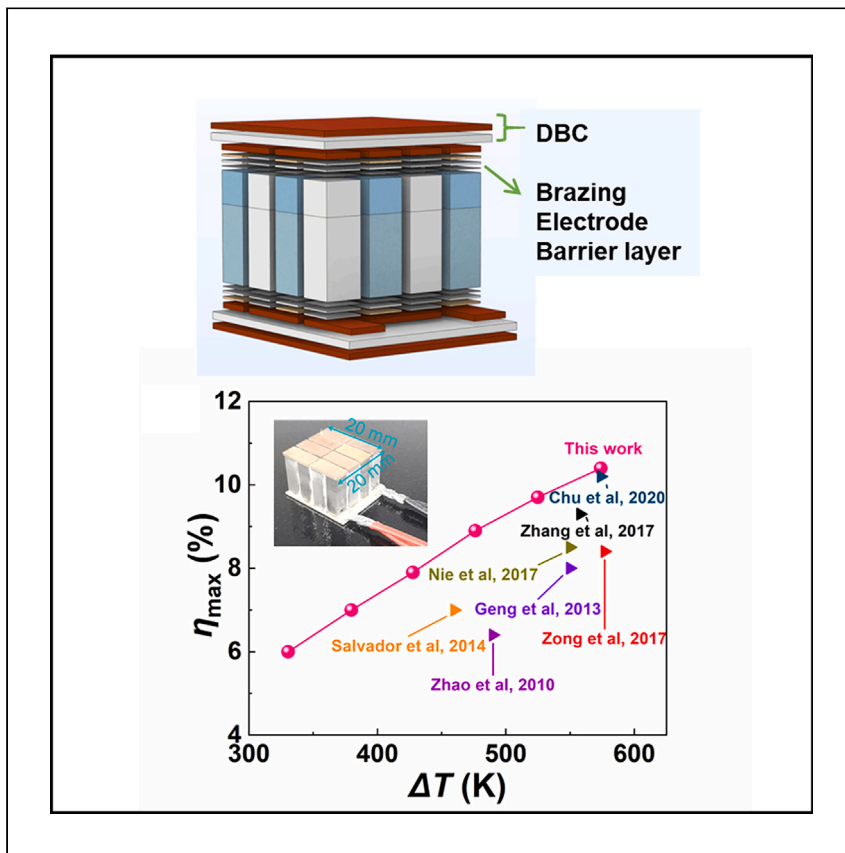
High-efficiency segmented thermoelectric power generation modules constructed from all skutterudites

Shun Wan, Qingfeng Song, Hongyi Chen, ..., Bin Chen, Shengqiang Bai, Lidong Chen

qihao.zhang@kit.edu (Q.Z.)
chenbin@hpstar.ac.cn (B.C.)

Highlights

Skutterudite-based segmented thermoelectric power generation module

One-step sintering for a segmented thermoelectric module

Fabricated same-parent module achieves conversion efficiency of 10.4%

Wan et al. demonstrate a full skutterudite-based segmented thermoelectric module with a module efficiency of 10.4%. The use of thermoelectric materials from the same parent avoids the difference in thermal expansion coefficients and compatibility factors. This work paves an effective approach to improve thermoelectric conversion efficiency and device reliability.

Report

High-efficiency segmented thermoelectric power generation modules constructed from all skutterudites

Shun Wan,[1,2,4,7] Qingfeng Song,[1,2,7] Hongyi Chen,[3] Qihao Zhang,[1,2,6,8,*] Jincheng Liao,[1,2] Xugui Xia,[1,2] Chao Wang,[1,2] Pengfei Qiu,[1,2] Bin Chen,[4,5,*] Shengqiang Bai,[1,2] and Lidong Chen[1,2]

SUMMARY

Development of thermoelectric conversion technology for power generation can alleviate the demand for fossil energy and increase the efficiency of energy utilization. To achieve more efficient heat-to-electric conversion, it is desirable to maximize the figure of merit (zT) over a wide temperature range. Constructing a segmented thermoelectric device by serially connecting materials with high zT at different operating temperatures has been proven feasible. However, the issue of compatibility of different thermoelectric materials and the method of connecting different segments to ensure high interfacial stability remain unsolved. Herein, we demonstrate a full skutterudite-based segmented thermoelectric power generation module. The use of thermoelectric materials from the same parent avoids the difference in thermal expansion coefficients and compatibility factors and allows the preparation of thermoelectric junctions by a one-step sintering process. As a result, a high module efficiency of 10.4% is obtained owing to the rational design of the materials, device geometry, and interfaces and is the highest value among skutterudite-based modules reported so far.

INTRODUCTION

Solid-state thermoelectric conversion technology based on the Seebeck effect for waste heat harvesting has been considered an alternative effective way to address the big challenge of the energy dilemma.[1–4] Ideally, the maximum conversion efficiency of a thermoelectric device depends on the material's average figure of merit (zT) value over the operating temperature range and the available temperature difference across the device. Therefore, in order to achieve a more efficient thermal-to-electric conversion, it is desirable to maximize zT over a larger temperature range. Over the past decades, a great amount of research has been devoted to improving the performance of thermoelectric materials, pushing the peak zT above 2.0 and even breaking the previously unheard-of level of 3.0.[5–14] However, high zT values for a given thermoelectric material always fall within a narrow temperature range (typically 100–300 K). Once outside this temperature range, zT drops rapidly, yielding a low average zT. So far, there is virtually no a single material that can maintain high zT values over its whole service temperature range.

An effective way to promote the average zT values over a wide temperature range is to construct a segmented thermoelectric device, that is, to use thermoelectric materials with different optimal operating temperatures along a temperature gradient and combine them into electrical series.[15–19] This segmented structure allows

[1]State Key Laboratory of High Performance Ceramics and Superfine Microstructure, Shanghai Institute of Ceramics, Chinese Academy of Sciences, Shanghai 200050, China

[2]Center of Materials Science and Optoelectronics Engineering, University of Chinese Academy of Sciences, Beijing 100049, China

[3]College of Chemistry and Chemical Engineering, Central South University, Changsha 410083, Hunan, China

[4]Center for High Pressure Science and Technology Advanced Research (HPSTAR), Shanghai 201203, China

[5]School of Science, Harbin Institute of Technology, Shenzhen 518055, China

[6]Present address: Light Technology Institute, Karlsruhe Institute of Technology, 76131 Karlsruhe, Germany

[7]These authors contributed equally

[8]Lead contact

*Correspondence: qihao.zhang@kit.edu (Q.Z.), chenbin@hpstar.ac.cn (B.C.)

https://doi.org/10.1016/j.xcrp.2023.101651

each different thermoelectric material to operate in its own favorable operating temperature range, consequently maximizing the average zT throughout the whole operating temperature range and effectively improving the device efficiency. In this case, Bi_2Te_3-based materials are usually chosen as the low-temperature segmented section because they possess by far the best thermoelectric properties around room temperature. Those materials such as filled skutterudite, GeTe, and PbTe with peak zT at ~800 K are ideal segmented sections for intermediate temperatures. SiGe-based and LaTe-based thermoelectric materials are excellent candidates at a higher temperature range of 850–1,100 K.[20–24]

To date, high conversion efficiencies ($\geq 12\%$) have been achieved in devices such as bismuth telluride/skutterudite segmented modules and bismuth telluride/high-entropy-stabilized chalcogenide segmented modules by fully considering the optimal thermoelectric properties as well as the rational device design.[7,19] However, there still exist problems, such as the reliability and stability of the segmented devices, that need to be addressed. For the evaluation and application of thermoelectric devices, reliability and stability are crucial, in addition to efficiency. In this regard, factors including device structural stability and material degradation during long-term service as well as the thermal expansion coefficient matching between different components are important in the development of thermoelectric devices. From this point of view, existing segmented thermoelectric devices fabricated from different kinds of thermoelectric materials suffer from some disadvantages. First, the mismatch of thermal expansion coefficients of two different adjacent thermoelectric materials may lead to the instability of the devices, especially interface failure during thermal cycling. Second, it is usually needed to design complex interfaces such as barrier layers to avoid elemental diffusion between different thermoelectric materials. These interfacial barrier materials may increase the interfacial electrical resistances and thermal resistances, resulting in interfacial energy loss and the reduction of conversion efficiency. In addition, the preparation of thermoelectric junctions of these segmented materials usually requires complex processes such as soldering. The fabrication process is complicated by the fact that one-step sintering cannot be used because of the different sintering temperatures of the different thermoelectric materials.

In view of these drawbacks, segmented thermoelectric devices using the same kind of thermoelectric materials could be a possible solution. Carrier concentration gradient function thermoelectric devices were developed by manipulating the carrier concentration gradients throughout one thermoelectric material via the Bridgman technique, the Czochralski technique, or the unidirectional solidification method, which leads to the shift of the zT peak to higher or lower temperatures.[25–29] For example, indium-doped PbTe-based crystals were prepared by the Czochralski technique. As a result, the Seebeck coefficient keeps practically constant value over a wide temperature range. However, the length of the sample with a graded charge carrier concentration relies on many factors such as the diffusion source and treatment temperature. This makes the design of the final modules uncontrollable and inflexible. In addition, the diffusion of impurities between different layers can easily cause the decline of thermoelectric properties by the unidirectional solidification method.

To overcome the above challenges, we herein construct a segmented thermoelectric power generation module by using all skutterudite-based materials. The n-type leg consists of $In_{0.25}Co_4Sb_{12}$ and $Yb_{0.35}Co_4Sb_{12}$, while the p-type leg consists of $Ce_{0.9}Fe_3CoSb_{12}$ and $CeFe_{3.85}Mn_{0.15}Sb_{12}$. A one-step sintering process is used to prepare the all-$CoSb_3$-based junctions, which simplifies the fabrication process of
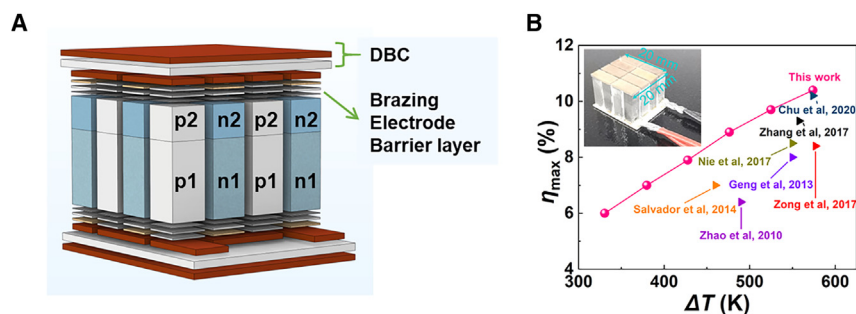
Figure 1. Development of segmented skutterudite thermoelectric modules for higher efficiency

(A) Schematic diagram of a segmented thermoelectric module fabricated using the same kind of thermoelectric materials.

(B) Comparison of the conversion efficiency of the full skutterudite-based segmented module with previous skutterudite modules.[19,30–35] Inset is the optical image of an 8-pair segmented skutterudite module fabricated in this work.

segmented modules. In addition, the problems of elemental diffusion and mismatching coefficients of thermal expansion between different segmented section materials are easily solved through the segmentation design of same-parent skutterudites. Through further geometrical optimization, we successfully obtain a measured module efficiency of 10.4% under a temperature gradient of 574 K (Figure 1).

RESULTS AND DISCUSSION

Materials selection and design of full skutterudite-based segmented modules

When selecting the materials of each segmented section in the temperature range for a segmented thermoelectric device, several design factors should be considered. First, the average zT of the selected materials should be the highest in this temperature range. $CoSb_3$-based skutterudite materials are considered one of the best thermoelectric materials for intermediate temperature applications. Over the last 20 years, researchers of skutterudite-based materials have mainly aimed to increase the highest zT values, mostly at temperatures above 700 K. Thus, skutterudites with excellent thermoelectric properties at a low temperature range are needed to fabricate a full skutterudite-based segmented module. Figure 2A presents the temperature-dependent zT of n-type and p-type skutterudites used in this work. It is found that n-type $In_{0.25}Co_4Sb_{12}$ possesses higher zT values at a low temperature range (<700 K), while n-type $Yb_{0.35}Co_4Sb_{12}$ possesses higher zT values at a high temperature range (>700 K). The average zT value of $In_{0.25}Co_4Sb_{12}$ is 15% higher than that of $Yb_{0.35}Co_4Sb_{12}$ at 300–700 K. Thus, $In_{0.25}Co_4Sb_{12}$ and $Yb_{0.35}Co_4Sb_{12}$ can be used as the low-temperature and high-temperature segmented sections for the combination of n-type thermoelectric legs. Similarly, $Ce_{0.9}Fe_3CoSb_{12}$ and $CeFe_{3.85}Mn_{0.15}Sb_{12}$ are identified as the low-temperature and high-temperature segmented sections for the combination of p-type thermoelectric legs because of their high average zT at a low temperature range (<700 K) and a high temperature range (<700 K), respectively. The thermoelectric properties of all n-type and p-type skutterudites used in this work are reproducible during the mass production fabrication, and large-sized bulk samples with typical dimensions of 30 mm in diameter and 12 mm in height were prepared by hot-press sintering (Figure S1).

The second design factor for the segmented section selection is the coefficients of thermal expansion (CTE) consideration. Figure 2B presents the CTE value of typical n-type and p-type thermoelectric materials at room temperature. Both the n-type and p-type skutterudites used in this work possess close CTEs compared with other types of
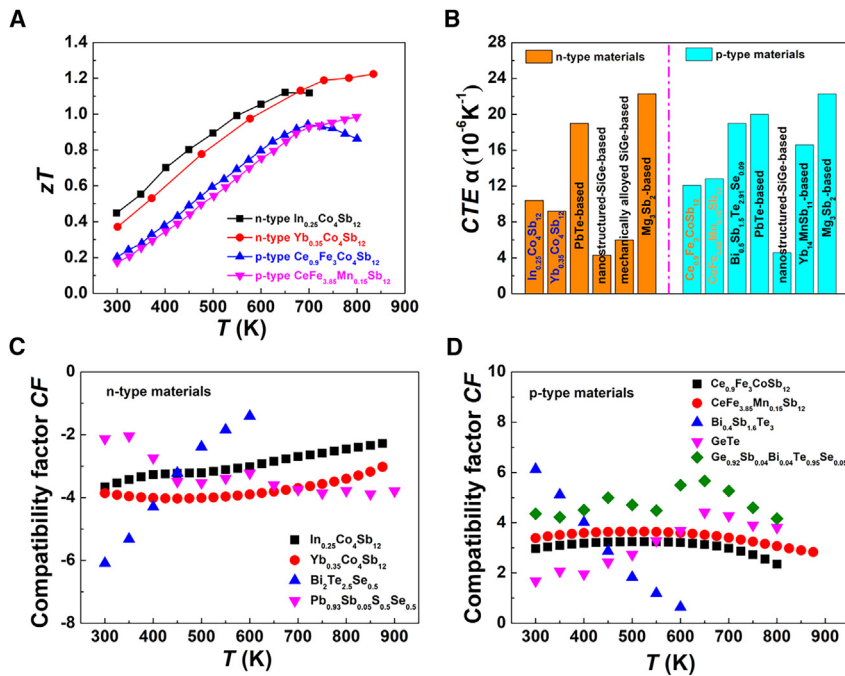
Figure 2. Thermoelectric properties of skutterudite materials

(A) Temperature-dependent zT of n-type and p-type skutterudites in this work.

(B) Coefficient of thermal expansion of several typical n-type and p-type thermoelectric materials. Some data were taken from Agne et al.,[36] Drasar and Müller,[37] Ferreres et al.,[38] Hikage et al.,[39] and Ravi et al.[40] for comparison.

(C) Calculated compatibility factor (CF) of several n-type thermoelectric materials.

(D) Calculated CF of several p-type thermoelectric materials. Data of thermoelectric properties of skutterudites are from materials measured in this work, and data of other materials are taken from Zhang et al.[19] and Xing et al.[41]

thermoelectric materials. Moreover, the temperature-dependent CTEs of both the n-type and p-type skutterudites also possess similar values at 300–900 K (Figure S2).

Finally, the compatibility factor (CF) can be expressed by $CF = \frac{\sqrt{1+ZT}-1}{ST}$, where S is the Seebeck coefficient, which also needs to be considered in order to ensure maximum efficiency of thermoelectric generation,[42–45] and T is the absolute temperature. The CFs of several n-type and p-type thermoelectric materials were calculated and are shown in Figures 2C and 2D. It is found that the n-type and p-type skutterudites used in this work possess the most similar CFs compared with other n-type or p-type thermoelectric materials.

As mentioned above, n-type filled skutterudites of $In_{0.25}Co_4Sb_{12}$ and $Yb_{0.35}Co_4Sb_{12}$ were finally used as the low-temperature and high-temperature segmented sections for the combination of the n-type leg of the module, respectively, while the p-type filled skutterudites of $Ce_{0.9}Fe_3CoSb_{12}$ and $CeFe_{3.85}Mn_{0.15}Sb_{12}$ were used as the low-temperature and high-temperature segmented sections for the combination of the p-type leg of the module, respectively.

Interfacial properties of skutterudite-based segmented junctions

The full skutterudite-based segmented legs can be obtained by one-step sintering, without the soldering process used in Bi_2Te_3-based materials and skutterudite-based materials. As shown in Figures 3A and 3C, scanning electron microscopy
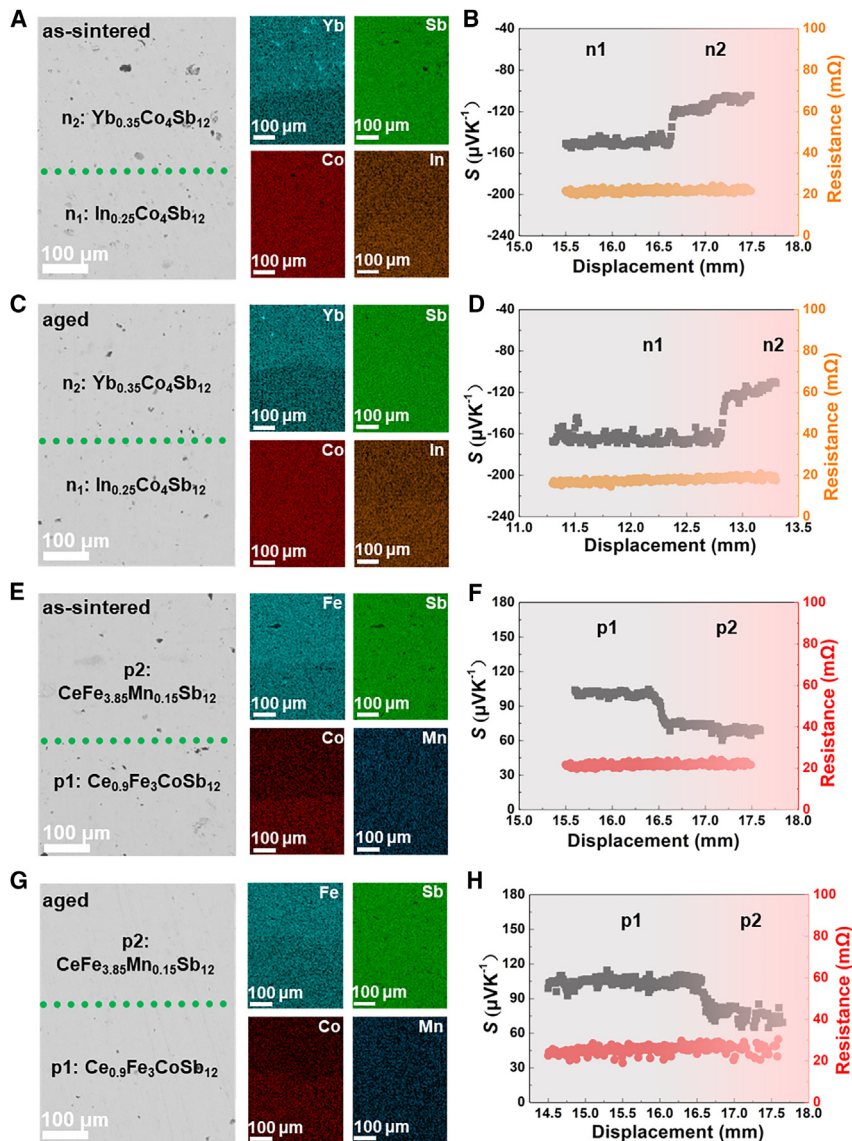
**Figure 3. Thermal stability of segmented skutterudite interfaces**

(A and C) SEM image and EDS element mapping of n-type $In_{0.25}Co_4Sb_{12}/Yb_{0.35}Co_4Sb_{12}$ junctions (A) as-sintered and (C) after thermal aging at 723 K for 360 h.

(B and D) Measured scanning Seebeck coefficient and resistance of n-type $In_{0.25}Co_4Sb_{12}/Yb_{0.35}Co_4Sb_{12}$ junctions as function of probe displacement (B) as-sintered and (D) after thermal aging at 723 K for 360 h.

(E and G) SEM image and EDS element mapping of p-type $Ce_{0.9}Fe_3CoSb_{12}/CeFe_{3.85}Mn_{0.15}Sb_{12}$ junctions (E) as-sintered and (G) after thermal aging at 723 K for 360 h.

(F and H) Measured scanning Seebeck coefficient and resistance of p-type $Ce_{0.9}Fe_3CoSb_{12}/CeFe_{3.85}Mn_{0.15}Sb_{12}$ junctions (F) as-sintered and (H) after thermal aging at 723 K for 360 h.

(SEM) and energy-dispersive spectroscopy (EDS) were employed to investigate the interface of n-type $In_{0.25}Co_4Sb_{12}/Yb_{0.35}Co_4Sb_{12}$ junctions before and after annealing at 723 K for 360 h in vacuum. It can be seen that there is no obvious diffusion even after annealing, indicating that the interface is stable during the thermal aging process. The interfacial contact resistances of n-type $In_{0.25}Co_4Sb_{12}/Yb_{0.35}Co_4Sb_{12}$ junctions before and after annealing at 723 K for 360 h were measured by a four-probe method along with the scanning Seebeck coefficient. As presented in
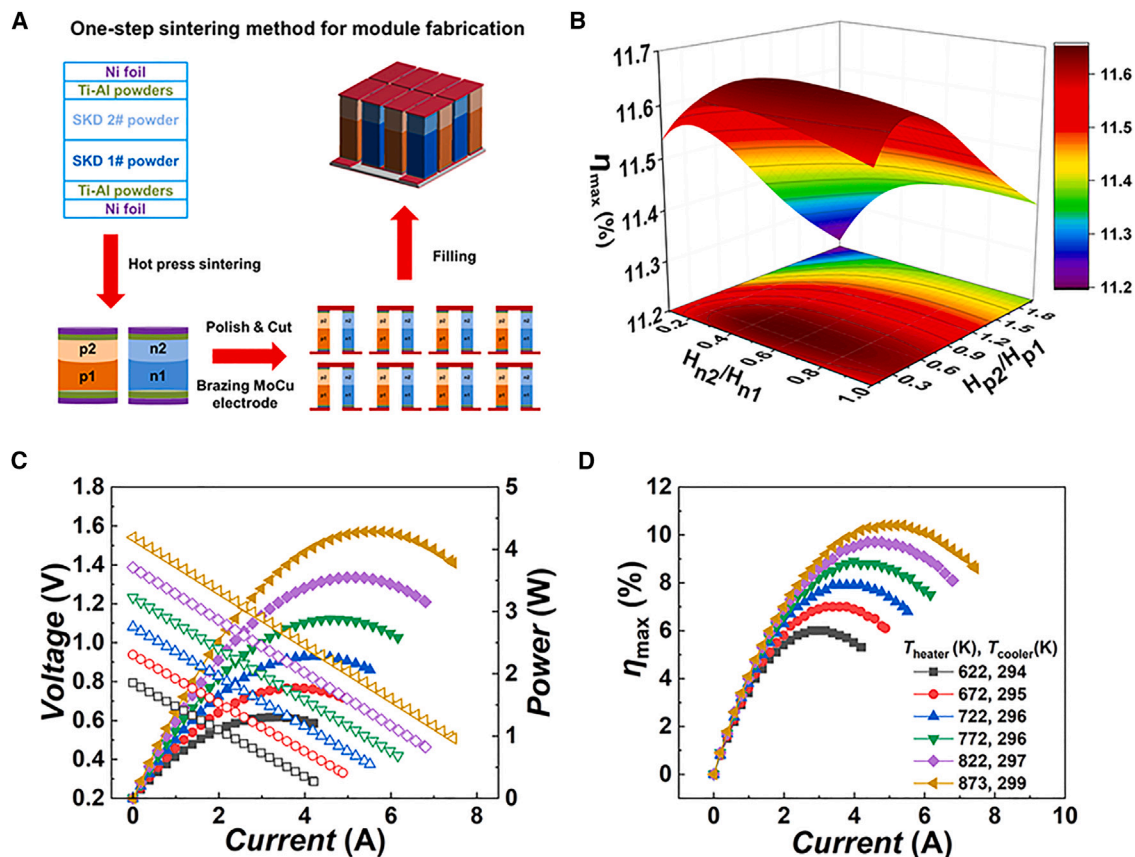
Figure 4. Power-generating performance of segmented skutterudite thermoelectric modules
(A) One-step sintering method to fabricate segmented skutterudite junctions.
(B) 3D plots relating simulated maximum conversion efficiency (η_{max}) with the segment height ratio.
(C and D) Measured output voltage V (hollows) and output power P (solids) (C) and η_{max} of the segmented skutterudite module as a function of current I (D) under different operating temperatures.

Figures 3B and 3D, there are obvious jump points in the Seebeck coefficient, corresponding to the position of $In_{0.25}Co_4Sb_{12}/Yb_{0.35}Co_4Sb_{12}$ interface, while there are no apparent jump points in the resistance. Similar results are obtained in the p-type $Ce_{0.9}Fe_3CoSb_{12}/CeFe_{3.85}Mn_{0.15}Sb_{12}$ junctions. As shown in Figures 3E–3H, there are almost no contact resistances observed at the skutterudite interfaces. The enlarged figures of n-type and p-type junctions are presented in Figure S3 to show the high-resolution scan plot around the junctions. Even after thermal aging at 723 K for 360 h, the contact resistances are still negligible. In addition, the nearly identical CTEs for each segmented composition could ensure high device durability.

Geometry design, fabrication, and evaluation of segmented skutterudite modules

Based on the simulated results, we fabricated the full skutterudite-based segmented modules (Figure 4A). The optical image of the fabricated 8-pair full skutterudite-based segmented module is shown in Figure 1B. A 3D finite-element model was obtained by a full parameter optimization based on the measurement transport properties of each material.[19] The interfacial contact resistances were also considered during the simulation process. As shown in Figure 4B, the maximum conversion efficiency (η_{max}) initially rises and then falls with increasing the ratio of the length of the high-temperature segmented section and the low-temperature segmented

section. The corresponding voltage distribution and temperature distribution when the η_{max} is obtained are shown in Figure S4. Based on the simulations, we finally confirmed the actual length of each composition. Specifically, the η_{max} reaches up to 11.6% at the optimized dimensions of $H_{n2}/H_{n1} = 0.4$ for the n-type leg and $H_{p2}/H_{p1} = 0.5$ for the p-type leg at a hot-side temperature (T_{heater}) of 873 K and a cold-side temperature (T_{cooler}) of 300 K.

Figure 4C presents the measured current (I)-dependent output voltage (V) and output power (P) at different temperature difference for the fabricated 8-pair full skutterudite-based segmented module. The open-circuit voltage (V_{oc}) and the internal resistance of the module (R_{in}) could be obtained from the intercept and slope of the current-dependent output voltage curves, respectively. A maximum power output (P_{max}) of 4.3 W is reached at a hot-side temperature of 873 K and a ΔT of 574 K. An η_{max} of 10.4% is achieved at a hot-side temperature of 873 K and acold-side temperature of 299 K (Figure 4D) for the fabricated 8-pair full skutterudite-based segmented module. There is a discrepancy between the measured and simulated efficiency, which is mainly due to the heat loss caused by the radiation from the heat source at high temperatures.[19] Even so, the measured efficiency is the highest value among all full skutterudite-based modules ever reported (Figure 1B), which is attributed to the higher average zT of each segmented section as well as the low-resistance interface resulting from the junction with the same kind of material.

In this work, the module structure design and the interface design for a full skutterudite-based thermoelectric segmented module were achieved. The fabricated 8-pair skutterudite module achieves a conversion efficiency of 10.4% at a hot-side temperature of 873 K and a ΔT of 574 K. The high efficiency of this power generation module was attributed to the combined rational design strategy of both the selective n- and p-type materials as well as effective interfaces. This work paves an adaptable and effective approach to improve the thermoelectric conversion efficiency of a power generation module by rational design of the segmented legs as well as the interface.

EXPERIMENTAL PROCEDURES

Resource availability

Lead contact
Further information and requests for resources should be directed to and will be fulfilled by the lead contact, Qihao Zhang (qihao.zhang@kit.edu).

Materials availability
All unique/stable reagents generated in this study are available from the lead contact upon reasonable request with a completed materials transfer agreement.

Data and code availability
The data that support the findings of this study are available from the corresponding authors upon reasonable request.

Materials synthesis
In this work, n-type filled skutterudites of $In_{0.25}Co_4Sb_{12}$ and $Yb_{0.35}Co_4Sb_{12}$ were used as the low-temperature and high-temperature segmented sections for the combination of the n-type leg of the module, respectively. P-type filled skutterudites of $Ce_{0.9}Fe_3CoSb_{12}$ and $CeFe_{3.85}Mn_{0.15}Sb_{12}$ were used as the low-temperature and high-temperature segmented sections for the combination of the p-type leg of

the module, respectively. The n-type and p-type filled skutterudite powders used for the module were fabricated according to the processes described in our previous work.[19] Briefly, high-purity raw materials including In (shot, 99.9999%), Yb (ingot, 99.9%), Co (shot, 99.95%), Sb (shot, 99.9999%), Ce (ingot, 99.9%), Fe (pieces, 99.99%), and Mn (pieces, 99.95%) were weighed according to the nominal compositions of the selected skutterudites and then sealed into quartz tubes after pumping. The quartz tubes were slowly heated to 1,373 K, kept at this temperature for 20 h, and then quenched in a water bath. Then, the quartz tubes were annealed at 993 K for 168 h for n-type skutterudites of $In_{0.25}Co_4Sb_{12}$ and $Yb_{0.35}Co_4Sb_{12}$. On the other hand, the quartz tubes were annealed at 973 K for 168 h for the p-type filled skutterudites of $Ce_{0.9}Fe_3CoSb_{12}$ and $CeFe_{3.85}Mn_{0.15}Sb_{12}$. The obtained ingots were ground into fine powders and sieved through a 200 mesh sieve.

Module fabrication

For module fabrication, n-type and p-type filled skutterudite powders were weighed according to their theoretical density and the designed dimension by ANSYS simulation. Typically, the lengths of n-type $In_{0.25}Co_4Sb_{12}$ and $Yb_{0.35}Co_4Sb_{12}$ are 8 and 4 mm, respectively. The lengths of p-type $Ce_{0.9}Fe_3CoSb_{12}$ and $CeFe_{3.85}Mn_{0.15}Sb_{12}$ are 8.5 and 3.5 mm, respectively. A Ni foil used for the cold-side electrode with a diameter of 30 mm was placed into a graphite die with a diameter of 30 mm. Then, $Ti_{88}Al_{12}$ powder with a thickness of 100 µm was uniformly spread onto the Ni foil. Afterward, the filled skutterudite powders were loaded onto the $Ti_{88}Al_{12}$, followed by another $Ti_{88}Al_{12}$ powder and Ni foil. Therefore, sandwich-structured Ni/$Ti_{88}Al_{12}$/segmented skutterudite/$Ti_{88}Al_{12}$/Ni joints can be obtained. A one-step hot-pressing sintering method was adopted to obtain the segmented thermoelectric legs. The sintering conditions were 953 and 913 K for n-type and p-type legs, respectively, with a heating rate of 50 K/min, a holding pressure of 65 MPa, and a holding time of 2 h.

The sintered n-type and p-type legs were then cut into rectangular blocks with a cross-sectional area of 4 × 4 mm. Eight n/p pairs were then positioned and soldered onto the copper-clad alumina ceramic plate to obtain the full skutterudite-based segmented modules. The detailed module fabrication process has been reported in our previous work.[19]

Module characterization

A SEM (ZEISS Supra 55) equipped with EDS was used to investigate the microstructures near the interfaces of each segmented section before and after the thermal aging test. Room temperature interfacial contact resistance along with the Seebeck coefficient scanning was performed with a Potential-Seebeck Microprobe (PSM; Panco GmbH). The details of module power-generating characterizations were similar to our previous work.[19] The output voltage, output power, and conversion efficiency were recorded in the temperature ramping process when the hot-side temperatures (T_h) reached 623, 673, 723, 773, 823, and 873 K, respectively. The measurement error of electrical conductivity, Seebeck coefficient, and thermal conductivity of thermoelectric materials are 5%, 5%, and 7%, respectively. The measurement error of conversion efficiency is 10%. The thermal aging condition for n-type $In_{0.25}Co_4Sb_{12}$/$Yb_{0.35}Co_4Sb_{12}$ junctions and p-type $Ce_{0.9}Fe_3CoSb_{12}$/$CeFe_{3.85}Mn_{0.15}Sb_{12}$ junctions was 723 K for 360 h in an Ar atmosphere. Note that we set the thermal aging temperature to 723 K because we needed to study the stability of the interfaces between the same-parent skutterudite materials. The interfacial stability between skutterudite and electrodes has been comprehensively studied in our previous work.[46]

SUPPLEMENTAL INFORMATION

Supplemental information can be found online at https://doi.org/10.1016/j.xcrp.2023.101651.

AUTHOR CONTRIBUTIONS

S.W. and Q.S. contributed equally to this work. This paper was written collaboratively by S.W., Q.S., H.C., Q.Z., P.Q., B.C., S.B., and L.C. with input from all other authors. Sample synthesis, structural characterization, and thermoelectric transport property measurements were performed by S.W. and Q.S. Module preparation and measurements were performed by S.W., Q.S., Q.Z., J.L., X.X., and C.W. Module numerical modeling was done by Q.Z. All authors contributed to the data analysis, discussed the results, and commented on the manuscript.

DECLARATION OF INTERESTS

The authors declare no competing interests.

REFERENCES

1. He, J., and Tritt, T.M. (2017). Advances in thermoelectric materials research: looking back and moving forward. Science 357, eaak9997. https://doi.org/10.1126/science.aak9997.

2. Shi, X.L., Zou, J., and Chen, Z.G. (2020). Advanced thermoelectric design: from materials and structures to devices. Chem. Rev. 120, 7399–7515. https://doi.org/10.1021/acs.chemrev.0c00026.

3. Zhang, Q.H., Huang, X.Y., Bai, S.Q., Shi, X., Uher, C., and Chen, L.D. (2016). Thermoelectric devices for power generation: recent progress and future challenges. Adv. Eng. Mater. 18, 194–213. https://doi.org/10.1002/adem.201500333.

4. Zhu, T., Liu, Y., Fu, C., Heremans, J.P., Snyder, J.G., and Zhao, X. (2017). Compromise and synergy in high-efficiency thermoelectric materials. Adv. Mater. 29, 201605884. https://doi.org/10.1002/adma.201702816.

5. Fu, C., Bai, S., Liu, Y., Tang, Y., Chen, L., Zhao, X., and Zhu, T. (2015). Realizing high figure of merit in heavy-band p-type half-Heusler thermoelectric materials. Nat. Commun. 6, 8144. https://doi.org/10.1038/ncomms9144.

6. Han, C.G., Qian, X., Li, Q., Deng, B., Zhu, Y., Han, Z., Zhang, W., Wang, W., Feng, S.P., Chen, G., and Liu, W. (2020). Giant thermopower of ionic gelatin near room temperature. Science 368, 1091–1098. https://doi.org/10.1126/science.aaz5045.

7. Jiang, B., Yu, Y., Cui, J., Liu, X., Xie, L., Liao, J., Zhang, Q., Huang, Y., Ning, S., Jia, B., et al. (2021). High-entropy-stabilized chalcogenides with high thermoelectric performance. Science 371, 830–834. https://doi.org/10.1126/science.abe1292.

8. Liu, H., Shi, X., Xu, F., Zhang, L., Zhang, W., Chen, L., Li, Q., Uher, C., Day, T., and Snyder, G.J. (2012). Copper ion liquid-like thermoelectrics. Nat. Mater. 11, 422–425. https://doi.org/10.1038/NMAT3273.

9. Mao, J., Zhu, H., Ding, Z., Liu, Z., Gamage, G.A., Chen, G., and Ren, Z. (2019). High thermoelectric cooling performance of n-type Mg3Bi2-based materials. Science 365, 495–498. https://doi.org/10.1126/science.aax7792.

10. Pei, Y., Shi, X., LaLonde, A., Wang, H., Chen, L., and Snyder, G.J. (2011). Convergence of electronic bands for high performance bulk thermoelectrics. Nature 473, 66–69. https://doi.org/10.1038/nature09996.

11. Shi, X., Yang, J., Salvador, J.R., Chi, M., Cho, J.Y., Wang, H., Bai, S., Yang, J., Zhang, W., and Chen, L. (2011). Multiple-filled skutterudites: high thermoelectric figure of merit through separately optimizing electrical and thermal transports. J. Am. Chem. Soc. 133, 7837–7846. https://doi.org/10.1021/ja211185w.

12. Zhang, J., Song, L., Madsen, G.K.H., Fischer, K.F.F., Zhang, W., Shi, X., and Iversen, B.B. (2016). Designing high-performance layered thermoelectric materials through orbital engineering. Nat. Commun. 7, 10892. https://doi.org/10.1038/ncomms10892.

13. Zhao, L.D., Lo, S.H., Zhang, Y., Sun, H., Tan, G., Uher, C., Wolverton, C., Dravid, V.P., and Kanatzidis, M.G. (2014). Ultralow thermal conductivity and high thermoelectric figure of merit in SnSe Crystals. Nature 508, 373–377. https://doi.org/10.1038/nature13184.

14. Zhao, W., Liu, Z., Sun, Z., Zhang, Q., Wei, P., Mu, X., Zhou, H., Li, C., Ma, S., He, D., et al. (2017). Superparamagnetic enhancement of thermoelectric performance. Nature 549, 247–251. https://doi.org/10.1038/nature23667.

15. Hong, M., Zheng, K., Lyv, W., Li, M., Qu, X., Sun, Q., Xu, S., Zou, J., and Chen, Z.G. (2020). Computer-aided design of high-efficiency GeTe-based thermoelectric devices. Energy Environ. Sci. 13, 1856–1864. https://doi.org/10.1039/d0ee01004a.

16. Jaziri, N., Boughamoura, A., Müller, J., Mezghani, B., Tounsi, F., and Ismail, M. (2020). A comprehensive review of Thermoelectric Generators: Technologies and common

applications. Energy Rep. 6, 264–287. https://doi.org/10.1016/j.egyr.2019.12.011.

17. Xing, Y., Liu, R., Liao, J., Zhang, Q., Xia, X., Wang, C., Huang, H., Chu, J., Gu, M., Zhu, T., et al. (2019). High-efficiency half-Heusler thermoelectric modules enabled by self-propagating synthesis and topologic structure optimization. Energy Environ. Sci. 12, 3390–3399. https://doi.org/10.1039/c9ee02228g.

18. Xu, C., Liang, Z., Ren, W., Song, S., Zhang, F., and Ren, Z. (2022). Realizing high energy conversion efficiency in a novel segmented-$Mg_3(Sb,Bi)_2$/Cubic-GeTe thermoelectric module for power generation. Adv. Energy Mater. 12, 2202392. https://doi.org/10.1002/aenm.202202392.

19. Zhang, Q., Liao, J., Tang, Y., Gu, M., Ming, C., Qiu, P., Bai, S., Shi, X., Uher, C., and Chen, L. (2017). Realizing a thermoelectric conversion efficiency of 12% in bismuth telluride/skutterudite segmented modules through full-parameter optimization and energy-loss minimized integration. Energy Environ. Sci. 10, 956–963. https://doi.org/10.1039/C7EE00447H.

20. El-Genk, M.S., and Saber, H.H. (2005). Performance analysis of cascaded thermoelectric converters for advanced radioisotope power systems. Energy Convers. Manag. 46, 1083–1105. https://doi.org/10.1016/j.enconman.2004.06.019.

21. El-Genk, M.S., Saber, H.H., and Caillat, T. (2003). Efficient segmented thermoelectric unicouples for space power applications. Energy Convers. Manag. 44, 1755–1772. https://doi.org/10.1016/S0196-8904(02)00217-0.

22. Gaurav, K., and Pandey, S.K. (2017). Efficiency calculation of a thermoelectric generator for investigating the applicability of various thermoelectric materials. J. Renew. Sustain. Energy 9, 014701. https://doi.org/10.1063/1.4976125.

23. Ouyang, Z., and Li, D. (2018). Design of segmented high-performance thermoelectric generators with cost in consideration. Appl. Energy 221, 112–121. https://doi.org/10.1016/j.apenergy.2018.03.106.

24. Liu, R., Xing, Y., Liao, J., Xia, X., Wang, C., Zhu, C., Xu, F., Chen, Z.G., Chen, L., Huang, J., and Bai, S. (2022). Thermal-inert and ohmic-contact interface for high performance half-Heusler based thermoelectric generator. Nat. Commun. 13, 7738. https://doi.org/10.1038/s41467-022-35290-6.

25. Cramer, C.L., Wang, H., and Ma, K. (2018). Performance of functionally graded thermoelectric materials and devices: a Review. J. Electron. Mater. 47, 5122–5132. https://doi.org/10.1007/s11664-018-6402-7.

26. Dariel, M.P., Dashevsky, Z., Jarashnely, A., Shusterman, S., and Horowitz, A. (2002). Carrier concentration gradient generated in p-type PbTe crystals by unidirectional solidification. J. Cryst. Growth 234, 164–170. https://doi.org/10.1016/S0022-0248(01)01660-8.

27. Dashevsky, Z., Shusterman, S., Dariel, M.P., and Drabkin, I. (2002). Thermoelectric efficiency in graded indium-doped PbTe crystals. J. Appl. Phys. 92, 1425–1430. https://doi.org/10.1063/1.1490152.

28. Hedegaard, E.M.J., Mamakhel, A.A.H., Reardon, H., and Iversen, B.B. (2018). Functionally graded $(PbTe)_{1-x}(SnTe)_x$ thermoelectrics. Chem. Mater. 30, 280–287. https://doi.org/10.1021/acs.chemmater.7b04473.

29. Kuznetsov, V.L., Kuznetsova, L.A., Kaliazin, A.E., and Rowe, D.M. (2002). High performance functionally graded and segmented Bi_2Te_3-based materials for thermoelectric power generation. J. Mater. Sci. 37, 2893–2897. https://doi.org/10.1023/A:1016092224833.

30. Chu, J., Huang, J., Liu, R., Liao, J., Xia, X., Zhang, Q., Wang, C., Gu, M., Bai, S., Shi, X., and Chen, L. (2020). Electrode interface optimization advances conversion efficiency and stability of thermoelectric devices. Nat. Commun. 11, 2723. https://doi.org/10.1038/s41467-020-16508-x.

31. Geng, H., Ochi, T., Suzuki, S., Kikuchi, M., Ito, S., and Guo, J. (2013). Thermoelectric properties of multifilled skutterudites with La as the main filler. J. Electron. Mater. 42, 1999–2005. https://doi.org/10.1007/s11664-013-2501-7.

32. Nie, G., Suzuki, S., Tomida, T., Sumiyoshi, A., Ochi, T., Mukaiyama, K., Kikuchi, M., Guo, J.Q., Yamamoto, A., and Obara, H. (2017). Performance of skutterudite-based modules. J. Electron. Mater. 46, 2640–2644. https://doi.org/10.1007/s11664-016-4849-y.

33. Salvador, J.R., Cho, J.Y., Ye, Z., Moczygemba, J.E., Thompson, A.J., Sharp, J.W., Koenig, J.D., Maloney, R., Thompson, T., Sakamoto, J., et al. (2014). Conversion efficiency of skutterudite-based thermoelectric modules. Phys. Chem. Chem. Phys. 16, 12510–12520. https://doi.org/10.1039/c4cp01582g.

34. Zong, P.a., Hanus, R., Dylla, M., Tang, Y., Liao, J., Zhang, Q., Snyder, G.J., and Chen, L. (2017). Skutterudite with graphene-modified grain-boundary complexion enhances zT enabling high-efficiency thermoelectric device. Energy Environ. Sci. 10, 183–191. https://doi.org/10.1039/c6ee02467j.

35. Zhao, D., Tian, C., Tang, S., Liu, Y., Jiang, L., and Chen, L. (2010). Fabrication of a $CoSb_3$-based thermoelectric module. Mater. Sci. Semicond. Process. 13, 221–224. https://doi.org/10.1016/j.mssp.2010.10.016.

36. Agne, M.T., Imasato, K., Anand, S., Lee, K., Bux, S.K., Zevalkink, A., Rettie, A.J., Chung, D.Y., Kanatzidis, M.G., and Snyder, G.J. (2018). Heat capacity of Mg_3Sb_2, Mg_3Bi_2, and their alloys at high temperature. Mater. Today Phys. 6, 83–88. https://doi.org/10.1016/j.mtphys.2018.10.001.

37. Drasar, C., and Müller, E. (2005). Stacking of Bi_2Te_3 and $FeSi_2$ for thermoelectric applications. Mater. Sci. Forum 492–493, 273–280. https://doi.org/10.4028/www.scientific.net/MSF.492-493.273.

38. Ferreres, X.R., Aminorroaya Yamini, S., Nancarrow, M., and Zhang, C. (2016). One-step bonding of Ni electrode to n-type PbTe - a step towards fabrication of thermoelectric generators. Mater. Des. 107, 90–97. https://doi.org/10.1016/j.matdes.2016.06.038.

39. Hikage, Y., Masutani, S., Sato, T., Yoneda, S., Ohno, Y., Isoda, Y., Imai, Y., and Shinohara, Y. (2007). Thermal expansion properties of thermoelectric generating device component. In 26th International Conference on Thermoelectrics, pp. 331–335. https://doi.org/10.1109/ICT.2007.4569489.

40. Ravi, V., Firdosy, S., Caillat, T., Brandon, E., van der Walde, K., Maricic, L., and Sayir, A. (2011). Thermal expansion studies of selected high-temperature thermoelectric materials. J. Electron. Mater. 40, 1334–1442. https://doi.org/10.1007/s11664-010-1374-2.

41. Xing, T., Song, Q., Qiu, P., Zhang, Q., Gu, M., Xia, X., Liao, J., Shi, X., and Chen, L. (2021). High efficiency GeTe-based materials and modules for thermoelectric power generation. Energy Environ. Sci. 14, 995–1003. https://doi.org/10.1039/d0ee02791j.

42. Snyder, G.J., and Caillat, T. (2003). Using the compatibility factor to design high efficiency segmented thermoelectric generators. MRS Online Proc. Libr. 793, 118–123.

43. Snyder, G.J. (2004). Application of the compatibility factor to the design of segmented and cascaded thermoelectric generators. Appl. Phys. Lett. 84, 2436–2438. https://doi.org/10.1063/1.1689396.

44. Seifert, W., Müller, E., Snyder, G.J., and Walczak, S. (2007). Compatibility factor for the power output of a thermogenerator. Phys. Status Solidi 1, 250–252. https://doi.org/10.1002/pssr.200701181.

45. Yusuf, A., and Ballikaya, S. (2020). Modelling a segmented skutterudite-based thermoelectric generator to achieve maximum conversion efficiency. Appl. Sci. 10, 408. https://doi.org/10.3390/app10010408.

46. Zhang, Q., Liao, J., Tang, Y., Gu, M., Liu, R., Bai, S., and Chen, L. (2018). Interface stability of skutterudite thermoelectric materials/$Ti_{88}Al_{12}$. J. Inorg. Mater. 33, 889–894. https://doi.org/10.15541/jim20170517.